

Dispersible Conjugated Polymer Nanoparticles as Bio-Interface Materials for Label-Free Bacteria Detection

Nada El Giddawy^{1,2}, Shiwei Ren³, Abderrahim Yassar³, Alain Louis-Joseph⁴, H      Sauriat-Dorizon¹, Waleed M. A. El Rouby⁵, Ahmed O. El-Gendy⁶, Ahmed A. Farghali⁵, Hafsa Korri-Youssoufi^{1*}

¹ Universit   Paris-Saclay, CNRS, Institut de Chimie Mol  culaire et des Mat  riaux d'Orsay (ICMMO), ECBB, B  t 420, 2 Rue du Doyen Georges Poitou, 91400, Orsay, France

² Department of Biotechnology and Life Sciences, Faculty of Postgraduate Studies for Advanced Sciences (PSAS), Beni-Suef University, Beni-Suef, 62 511, Egypt

³ LPICM, CNRS, Ecole Polytechnique, Institut Polytechnique de Paris, route de Saclay, 91128 Palaiseau, France

⁴ PMC, CNRS, UMR 7643, Institut Polytechnique de Paris, route de Saclay, 91128 Palaiseau, France

⁵ Materials Science and Nanotechnology Department, Faculty of Postgraduate Studies for Advanced Sciences (PSAS), Beni-Suef University, Beni-Suef, 62 511, Egypt

⁶ Microbiology and Immunology Department, Faculty of Pharmacy, Beni-Suef University, Beni-Suef, Egypt

Abstract

Fast and efficient identification of bacterial pathogens in water and biological fluids is an important issue in medicine, food safety and public health concerns that requires low-cost and improved sensing strategies. Impedimetric sensors are promising tools for monitoring bacteria detection, due to their reliability and ease-of-use. We herein report a study on a new bio-interface-based amphiphilic poly(3-hexylthiophene)-b-poly(3-triethylene-glycol-thiophene), P3HT-*b*-P3TEGT, for label-free impedimetric detection of *Escherichia coli* (*E. coli*). This bio-interface is fabricated by self-assembly of P3HT-*b*-P3TEGT into core-shell nanoparticles, which are further decorated with mannose, leading to an easy-to-use solution-processable nanoparticle material for biosensing. The hydrophilic block, P3TEGT promotes antifouling and prevents non-specific interactions while improving the ionic and electronic transport properties, thus enhancing the electrochemical-sensing capability in aqueous solution. Self-assembly and micelle formation of P3HT-*b*-P3TEGT were analyzed by 2D-NMR, FTIR, DLS, contact angle and microscopy characterizations. Detection of *E. coli* was characterized and evaluated by electrochemical impedance spectroscopy, optical and scanning electron microscopy techniques. The sensing layer based on mannose-functionalized P3HT-*b*-P3TEGT nanoparticles demonstrates targeting ability toward *E. coli* pili protein with a detection range from 10³ CFU/mL to 10⁷ CFU/mL and selectivity studied with Gram(+)bacteria. Application to real samples was performed by detection of bacteria in tap water and Nile water. The approach developed here shows that water/alcohol-processable functionalized conjugated

polymer nanoparticles are suitable for use as electrode materials for the fabrication of a low-cost label-free impedimetric biosensor for the detection of bacteria in water.

Keywords: Bacteria, *E. coli* detection, biosensor, conjugated block copolymer, self-assembly, mannose, core-shell nanoparticle, impedimetric biosensor, conjugated polymer nanoparticle

1. Introduction

Rapid and sensitive detection of bacteria has become an urgent demand in the field of health care, food analysis, environmental monitoring, and security control to allow faster decisions to be made.¹ In order to develop a Point-of-Care system for rapid pathogen detection, it is critical to eliminate the time-consuming culture step and minimize sample preparation requirements. Thus, the need for real-time sensing and miniaturization into a portable, autonomous, and inexpensive platform is of utmost importance.^{2,3,4} To date, various classes of materials such as metal nanoparticles, carbon nanomaterials, self-assembled monolayers, and conducting polymers shown promise for electrochemical biosensing. There are many recent excellent reviews covering the field of existing electrochemical detection systems for bacteria with specific focus on the impedance-based detection of pathogenic bacteria⁵, nanomaterial-based electrochemical biosensors for pathogenic bacteria⁶, carbon nanomaterials⁷, including graphene and its various forms⁸, carbon nanotubes and their derivatives. Most of the sensors reported are in line with the main requirements for selectivity, sensitivity, and fast analysis, with a detection limit down to the level of few hundreds of colony forming units (CFU) per milliliter. Processable conjugated polymers (CPs) have been widely used as sensing materials in electrochemical sensors thanks to their unique electrical and electrochemical responses in the presence of different analytes.^{9, 10} The potential applications of CP materials in biosensors and biological applications have been reviewed extensively in the literature.^{11,12,13} Biosensing applications of CP require bioconjugation of receptor such as proteins, peptides, lipids, or carbohydrates in the polymeric system to afford specific targeting. Such bioconjugation techniques usually require the introduction of chemical functions, typically amine or carboxylic acid, and chemical control over the ligand functionalization of the CP via pre- or post-functionalization. Once immobilized, the biomolecules need to keep their original functionalities, so special attention must be

paid to the recognition site to ensure that it is not sterically hindered.¹¹ Covalent attachment is the method generally used for bioreceptor immobilization; this requires suitable functional groups on the CP to anchor the incoming biomolecule. However, the main disadvantage of this approach is that the immobilization of the bioreceptor on the CP surface changes its electronic and physical properties. Although covalent modification ensures robust and stable immobilization of biomolecules, this method is not compatible with CPs as it could degrade their intrinsic properties.¹¹ Non-covalent functionalization or physical entrapment is a relatively simple, fast and inexpensive immobilization process as compared to covalent modification.¹⁴

During the past decade, carbohydrates have been increasingly considered as alternative bioreceptors, as they are involved in key recognition events.¹⁵ In contrast to nucleic acids and antibodies, carbohydrates are more resistant to denaturation. Their small size offers also higher densities per unit surface area, which enhances the binding affinity.

Among them, mannose is a typical carbohydrate molecule that has good targeting ability towards *E. coli* pili on account of binding with the FimH lectin proteins.¹⁶ Mimicking the situations encountered on the cell surfaces during the initial recognition processes offers great promise in the development of biosensors for the detection of carbohydrate-binding proteins and pathogens.

Biosensors based on carbohydrate-functionalized π -conjugated polymers have quickly become a prominent research field, because of their high potential, as transducers for detecting bacteria, and carbohydrate-protein interactions.¹⁷ The key feature of biomolecule-functionalized CPs is that their electronic states are altered when bio-analytes are bound to receptors, producing fluorescence quenching. Using the fluorescence quenching mechanism, CPs have provided simple, sensitive, and colorimetric platforms for detecting proteins¹⁸, glycans¹⁹ and bacteria.²⁰ For example, soluble glyco-polythiophenes functionalized with sialic acid or mannose ligands were prepared and their ability to bind lectins, viruses, and bacteria was evaluated using a colorimetric readout.²¹ Cationic conjugated polymers have proven to be very useful for the detection and inactivation of pathogenic bacteria, thanks to interchain fluorescence resonance energy transfer.²² In addition to the use of CPs as fluorescent sensors, carbohydrate-functionalized conducting polymers have demonstrated high bio-electrochemical bacteria-sensing capability. Two approaches, post- and direct-functionalization, have been used to fabricate glycosylated CPs. For instance, Cosnier

et al. reported the electrochemical polymerization of pyrrole-3'-carbohydrate monomers and investigated the potential of these polymers for impedimetric detection of lectins, as label-free impedance sensors.²³ The drawback of this method is that it requires monomer synthesis. Additionally, the functional carbohydrate moieties induce steric hindrance, which may affect the chain-growth process during the electropolymerization. A second approach consists in synthesizing polymer scaffolds first. The carbohydrates are then introduced by means of click chemistry. Using this approach, Zeng et al. demonstrated the advantages of functionalized polythiophene, as a solid-state redox probe, and the well-established triazole-based coupling chemistry for incorporating a carbohydrate functionality to fabricate a new biointerface. This was characterized by differential pulse voltammetry, and showed excellent sensitivity and selectivity for Erythrina Cristagalli lectin analysis.²⁴ The same authors demonstrated the fabrication and validation of the mannosylated polythiophene bio-interface for the detection of the Gram(−) bacterium, *E. coli*. In their work, thiophene-containing fused quinone moieties were electropolymerized, and then coupled with a thiol-modified mannose, α -D-mannopyranoside. The glycol surface thus generated allowed label-free detection of two major bacterial cell surface biomarkers, the fimbriae proteins on bacterial pili and the lipopolysaccharides on Gram(−) bacteria using crystal microbalance and electrochemical readouts.²⁵ In all these cases, the CP has been chemically post- or direct-functionalized with relevant functions necessary to conjugate bio-specific ligands. While both these approaches have proven their efficiency, they often require extensive chemistry. Furthermore, the introduction of the required functional group alters, in the majority of cases, the intrinsic properties of the CP, such as conductivity, charge mobility, electroactivity and optoelectrical properties.

While electrochemical sensors have been widely studied in the academic literature, commercial applications have been hindered by several technical limitations such as low detection limit, non-specific adsorption issues, and low cost-effectiveness for mass production. **Developing materials adaptable for low cost production such** as printing technology could have benefit impact and has recently received substantial interest for electronic devices. To date, printing technologies have been implemented across a wide range of biomedical applications, including bio-electrochemical sensors.²⁶ Nevertheless, one of the biggest issues for printable

electronics is the availability of functional **biomaterials** that meet the demands of high performance, an ideal immobilization surface and an efficient signal transducer.²⁷ Water-dispersible conjugated polymer nanoparticles (CPNs) meet the requirements, such as easy processability, good ability for film formation and the presence on the surface of chemical functionality for bio-conjugation, are an effective approach to circumvent this challenge. Albeit CPNs are widely investigated as fluorescent probes in biomedical applications, cell imaging and biosensing, thanks to their versatile properties such as, narrow size dispersion, high brightness, biocompatibility and good photochemical stability.²⁸ To the best of our knowledge, there has been no report on the use of CPNs as solution-processable electrode materials for electrochemical biosensing.

In this work, a simple and versatile approach to prepare functionalized core-shell CPNs, **using eco-friendly solvent (i.e. alcohol)**, is presented. The functionalized CPNs were formed by the self-assembly of amphiphilic poly(3-hexylthiophene)-*block*-poly(3-triethylene glycol-thiophene) (P3HT-*b*-P3TEGT) and the well-established chemistry of micelles to decorate their surface with mannose, which is a carbohydrate that has a high affinity to bind efficiently to FimH adhesin of bacterial type 1 pili in *E. coli*, leading thus to fabricate an innovative bio-interface **with high surface ratio**. Finally, the mannose-functionalized bio-interface was validated for reagentless and label-free selective detection of *E. coli* by electrochemical impedance spectroscopy (EIS), Scheme 1. The advantages of using amphiphilic P3HT-*b*-P3TEGT are due to several features: (i) the P3HT block is responsible for π - π stacking, which drives the self-assembly behavior and mediates micelle formation, (ii) the hydrophilic P3TEGT block promotes the antifouling property and prevents non-specific interaction of other types of bacterial cells, (iii) the redox activity of the conjugated backbone is exploited as electrochemical transducer using EIS. It should be noted that a suitable choice of block sizes and PEG-chain length lead to the optimal sensing requirement, balancing the polarity needed for high electroactivity and antifouling properties to sense in aqueous medium with the hydrophobicity of P3HT block required to prevent film dissolution in aqueous electrolytes. The newly designed glycosylated bio-interface was successfully validated to detect *E. coli* via direct adhesion of the fimbriated *E. coli* onto the mannose immobilized P3HT-*b*-P3TEGT surface. *E. coli* BL21 was used as a model Gram(−) bacterial analyte, in

order to demonstrate the proof of concept, and Gram(+) bacteria, *Lactobacillus acidophilus* (ATCC 4356) were tested for selectivity. As a result, the new bio-interface formed by mannose embedded with CPNs provides a bio-electronic interface able to selectively detect *E. coli* with a wide range of sensitivity. The biosensor was also validated for detection of bacteria in tap water and water from the Nile to demonstrate its usefulness in real applications.

Scheme 1. Cartoon representation of self-assembly of P3HT-*b*-P3TEGT, mannose-functionalized CPNs and label-free impedimetric sensor for *E. coli* detection. Top: chemical structure of P3HT-*b*-P3TEGT, aggregation of the P3HT blocks via π - π interaction in methanol, formation of core-shell micelles by precipitation of the P3HT block and good solubility of the P3TEGT block in methanol, and mannose-decorated P3HT-*b*-P3TEGT nanoparticles by non-covalent interactions between hydrophilic TEGT segments on the outer surface of the nanoparticles and hydroxyl groups of the mannose. Bottom: mannose-P3HT-*b*-P3TEGT film coated on the electrode surface, *E. coli* attachment via pili-mannose binding and label-free impedimetric detection.

2. Experimental section

2.1. Bacteria growth and culture conditions

Bacterial cells (*E. coli* BL21) were grown overnight at 37 °C on Lauria broth (LB) medium. The broth cultures were centrifuged and washed three times with phosphate buffer saline (PBS). The bacterial cell concentration was determined from the optical density (OD600) and correlated with colony counting after plating. Aliquots of the bacterial culture were diluted in PBS to obtain cell suspensions calibrated at 1.0×10^7 CFU/mL for the biosensing assays. The suspensions were stored at 4 °C until use. For selectivity, *Lactobacillus acidophilus* (ATCC 4356) was cultured in de Man, Rogosa and Sharpe (MRS) agar medium then suspended in PBS by the same procedure. Other materials used are described in SI.1.1.

2.2. Synthesis and self-assembly of P3HT-*b*-P3TEGT

The detailed protocol for the synthesis of the P3HT-*b*-P3TEGT, as well as the chemical structure of the monomers and copolymer, is shown in SI, Scheme S1. Briefly, the P3HT block was prepared by Grignard metathesis polymerization in the presence of Ni(dppp)Cl₂ as catalyst to obtain precursor polymer P3HT with a living

chain-end [29]. This macroinitiator was added to the chain-extended reaction solution of the triethylene glycol (TEG)-substituted thiophene monomer for formation of a diblock structure. The synthesis and chemical structure of the monomers and the P3HT-*b*-P3TEGT are described in SI (see SI.1.2 and Scheme S1). The obtained P3HT-*b*-P3TEGT was purified by sequential Soxhlet washing with methanol, hexane and chloroform. The chloroform fraction was then collected and evaporated to dryness to afford the desired copolymer with a moderate molecular weight. The molecular weights of the copolymer was determined using gel permeation chromatography (GPC) with tetrahydrofuran as eluent and polystyrene calibration, where number average molecular weight $M_n = 15\text{Kg/mol}$ and polydispersity index of 1.6 (see Figure S1C) For self-assembly studies and micelle formation, 0.05, 1, 5 mg of P3HT-*b*-P3TEGT was dissolved in 1 mL of THF and stirred at 60 °C in the dark for 2 h, the resulting copolymer solution was added to anhydrous methanol, selected as non-solvent at room temperature (SI.1.3, Scheme S2). Nanomicelle formation was followed by DLS and ^1H NMR, and characterized by contact angle, scanning electron microscopy (SEM) and transmission electron microscopy (TEM) techniques.

2.3. Mannose conjugation to P3HT-*b*-P3TEGT nanomicelles

P3HT-*b*-P3TEGT nanomicelles decorated with different amounts of mannose were prepared by a self-assembly process. P3HT-*b*-P3TEGT was dissolved at 1 mg/mL in THF, stirred at 300 rpm for 2 h at room temperature. A 5 mg/mL solution of mannose in methanol was prepared by vigorous vortex shaking. Blends of P3HT-*b*-P3TEGT with mannose were prepared by mixing volume of mannose and P3HT-*b*-P3TEGT solutions in different ratios at room temperature (SI.1.4, Scheme S3). These suspensions were sonicated for 2 min in order to achieve uniform-sized micelles and a distribution of mannose on the surface of the micelles. The self-assembled micelles were characterized by ^1H NMR, FTIR, SEM and contact angle measurements.

2.4. Biosensor fabrication and assessment of *E. coli* attachment

P3HT-*b*-P3TEGT/mannose electrodes were fabricated by drop casting. 8 μL of a solution of P3HT-*b*-P3TEGT/mannose was deposited on a glassy carbon electrode (GCE). The electrodes were annealed at 50 °C for 2 h, then rinsed with deionized (DI) water to remove excess mannose. In order to achieve a biosensor with improved performance, the ratio of mannose to P3HT-*b*-P3TEGT nanomicelles, annealing

temperature and time (See SI.3.2) were optimized. Three weight ratios of P3HT-*b*-P3TEGT to mannose (1:5, 2:5, and 3:5) were prepared and studied. This was followed by measuring the detection of *E. coli* by EIS (see SI.4.1).

Detection of *E. coli* was performed by dipping the modified GCE/P3HT-*b*-P3TEGT/mannose electrode into a solution containing various amounts of bacteria from 10^2 to 10^7 CFU/mL and incubated at room temperature for 1 h. The biosensor was then washed with DI water and EIS measurement was performed in sterilized PBS buffer solution. The reproducibility of the electrodes was tested by measuring the EIS of different sets.

For optical microscopy studies, films of P3HT, P3HT-*b*-P3TEGT and P3HT-*b*-P3TEGT/mannose were deposited onto glass substrates by spin coating at 2000 rpm/min for 60 s and dried at 50 °C for 2 h. The thicknesses of the films are in the range of 100 nm to 300 nm considering the concentration and rotational speed used. The copolymer-modified glass substrates were then incubated with *E. coli* (10^7 CFU/mL) for 1 h, then washed with DI water and examined by optical microscopy.

2.5. Instruments and characterization methods

The instruments used for the characterization are detailed in SI (See SI.1). Electrochemical measurements were performed using a Metrohm Autolab PGSTAT12 Potentiostat with a three-electrode system in which polymer-modified GCE is the working electrode, The counter-electrode is a Pt wire and Ag/AgCl is used as the reference electrode in a single-glass-compartment cell containing sterilized PBS buffer, pH 7.2, as electrolyte. Cyclic voltammetry (CV) experiments were performed at potentials ranging from 0 V to 0.8 V at a scan rate of 0.05 V/s for the characterization of the P3HT-*b*-P3TEGT electrodes. EIS was measured at -0.4 V using an alternating potential of 10 mV amplitude in the frequency range from 0.1 Hz to 100 kHz.

3. Results and discussion

3.1. Synthesis and characterization P3HT-*b*-P3TEGT nanomicelles

P3HT-*b*-P3TEGT was prepared according to the procedure reported in the literature.^{29,30} The molecular structure of the chloroform-soluble fraction was confirmed by ¹H-NMR and FTIR spectroscopy. The ¹H-NMR spectrum of P3HT-*b*-P3TEGT and its peak assignment, shown in Figure S1a, confirm the molecular

structure of the copolymer and diblock formation. From NMR analysis a degree of polymerization (n) of the P3HT block of $\sim n = 18-20$ was estimated.³¹ The block distribution was estimated by the integration of the ^1H -NMR spectra, and the results demonstrate that P3HT-*b*-P3TEGT consists of 70 mol% of 3-hexyl-thiophene and 30 mol% of thiophene units substituted with oxyethylene groups (comparing the integration peak of Hm and He, see Figure S1a). This ratio is very close to the feed ratio of the monomers used in the copolymerization. The FTIR spectrum of the copolymer shows the characteristic bands related to the two blocks of copolymer (see SI.2.1, Figure S2).

It is well known that the self-assembly of diblock copolymers in selective solvents produces core-shell micelles with different structures.^{32,33,34} The morphology and the form of the micelles are affected by the structure, length of each block and the solvent used.³⁴ THF and chlorinated solvents are good solvents for both blocks, while methanol is a non-solvent for the P3HT block but a good solvent for the P3TEGT block. In such a case, the block copolymer can self-assemble in the presence of methanol to form polymeric micelles. Thus, adding methanol would promote the aggregation of the P3HT blocks via strong π - π interactions, while the hydrophilic P3TEGT blocks are solvated by methanol.³⁴

The first indication of successful self-assembly and micelle formation of P3HT-*b*-P3TEGT was obtained from the ^1H and ^1H - ^1H NOESY NMR analysis. NMR spectra show that upon addition of a small amount of CD_3OD (10%) to a chloroform solution of P3HT-*b*-P3TEGT various modifications are observed: (i) gradual broadening of the aromatic and aliphatic proton signals; (ii) decrease in the intensity of the deshielded narrow aromatic peaks and (iii) new peaks. The modification is pronounced for high amount of CD_3OD added. At higher concentration of CD_3OD (30%) (top spectrum in Figure 1), the hyperfine structure disappears completely and the line width of the signals increases. Changes in line-shape, chemical shift, and line width, and the appearance of a new signal are observed. These modifications in the NMR spectra reflect π - π aggregation and micellization induced by the methanol. The broad ^1H line is a result of restricted molecular mobility of P3HT block chains, which stick together and form aggregates.

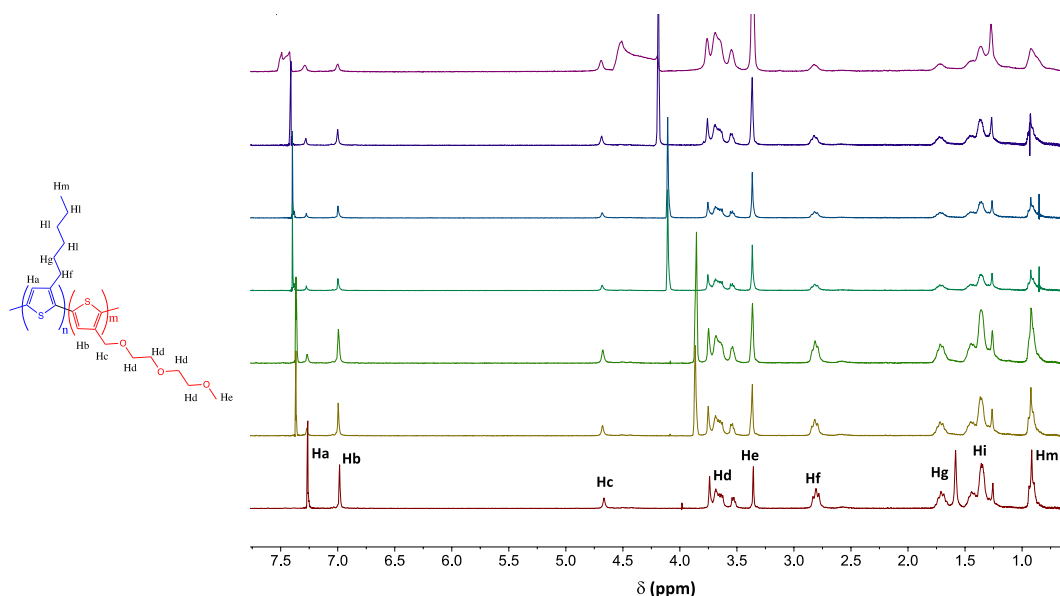


Figure 1. ^1H NMR of P3HT-*b*-P3TEGT (5 mg/ml CDCl_3) with successive addition of CD_3OD from bottom to top: 0, 0.1 ml, 0.15 ml, 0.2 ml, 0.25 ml, 0.3 ml, 0.4 ml.

2D NOESY NMR experiments were performed to better understand the self-assembly behavior of P3HT-*b*-P3TEGT. This technique allows the correlation of relatively close-range through-space proton-proton interactions.³⁵ The distance between alkyl group and thiophene ring protons is short enough to give NOE transfer. Thus, 2D NOESY experiments could give information on the self-assembly of the copolymer and the chemical core-shell structure of the nanomicelle. NOESY NMR spectra of P3HT-*b*-P3TEGT in CDCl_3 upon addition of CD_3OD were recorded (Figure 2, up). The spectrum in CDCl_3 with 5% of methanol- d_4 shows at least six cross-peaks between the thiophene ring and the hexyl group. The α -methylene protons at 2.6 ppm (labeled Hf) strongly interact with the aromatic proton of the thiophene ring in the P3HT block (labeled Ha) and interact also with β -methylene protons (labeled Hg) in the hexyl chain. Also, the spectrum shows that both the β -methylene protons and methylene protons in the hexyl chain (labeled Hi) strongly interact with the end methyl of the hexyl chain (labeled Hm). However, no NOE effects were observed between oxymethylene protons of the TEG segments; only the oxymethylene proton next to the thiophene ring (labeled Hc) interacts with the aromatic proton of thiophene in the P3TEGT block (labeled Hb). NOE is due to a dipole-dipole interaction through space, and it is sensitive to nuclei that are close together by bonding structures as well as the nuclei that are close together by (~ 0.5

nm).³⁶ The absence of an oxyethylene proton interaction is due to the large distance between chains, as observed by GIWAXS measurements.³⁷

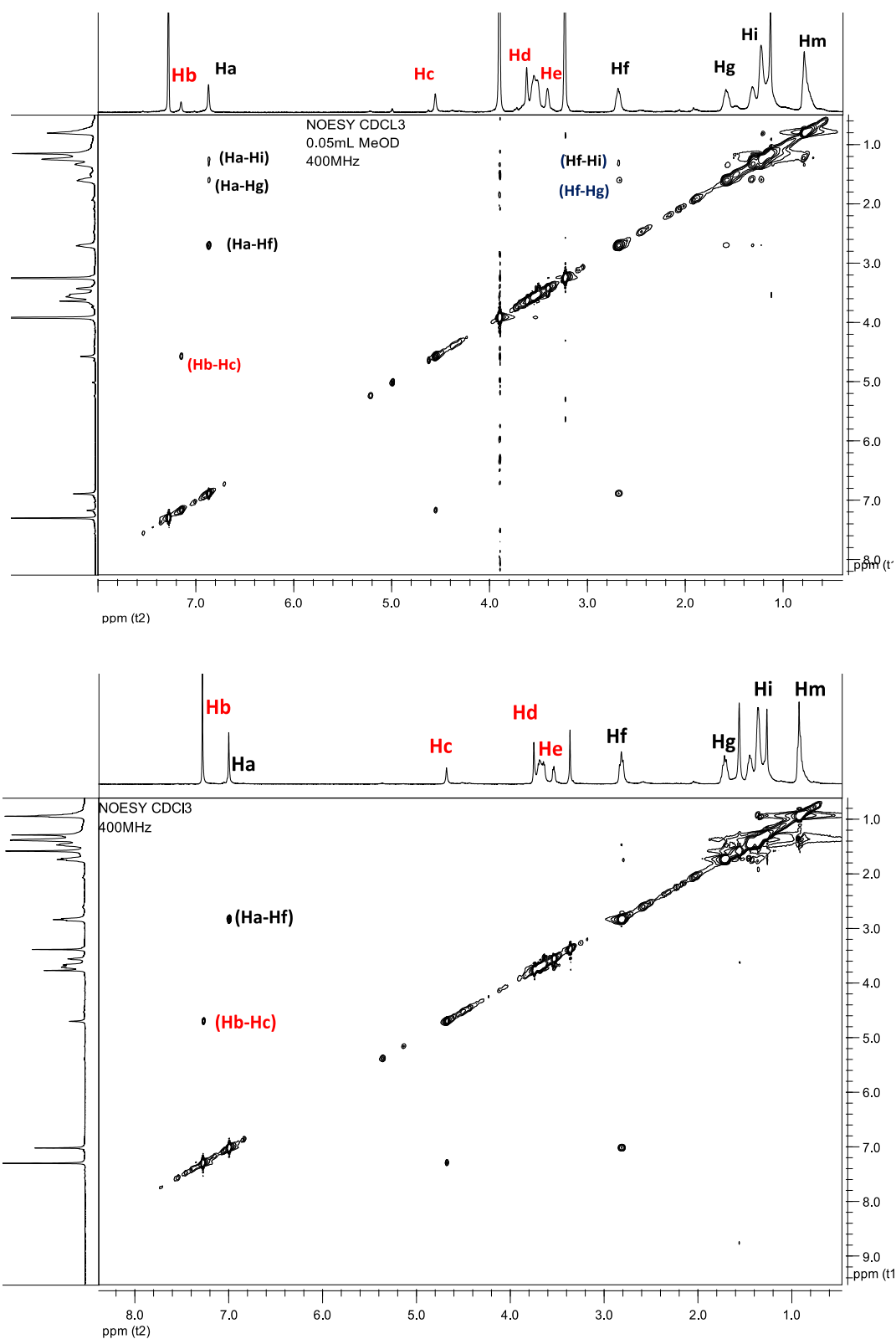


Figure 2. ^1H - ^1H NOESY NMR spectra of P3HT-*b*-P3TEGT in CDCl_3 with 5% of methanol- d_4 (up) and without CD_3OD (bottom)

Indeed, it has been demonstrated that the P3HT-*b*-P3TEGT self-assembly on lamellar structure and stacks with chain packing situations in the P3HT and P3TEGT phases, one with a d-spacing of 0.52 nm assigned to the mean inter-distance of the oxyethylene side groups between the P3TEGT block chains, while the other with d-spacing of 0.46 nm assigned to the mean inter-distance of the hexyl side groups between the P3HT block chains.³⁷ Therefore, the NOE is less sensitive to proton-proton-interaction of the TEGT side groups. These six cross-peaks indicate that the P3HT block is self-assembled in a lamellar π -stack structure. In this way, the hexyl chains of P3HT block are interdigitated between flanked highly ordered π -stacked aggregates (face-to-face) surrounded by domains of the hydrophilic P3HT blocks, core-shell nanomicelles. For comparison, we have analyzed the NOESY NMR spectrum of P3HT-*b*-P3TEGT in CDCl₃, before adding CD₃OD. It shows only two major cross-peaks (Figure 2, bottom). The α -methylene protons at 2.6 ppm strongly interact with the aromatic proton of the thiophene ring in the P3HT block, and the oxymethylene protons next to the thiophene ring interact with the aromatic proton of thiophene in the P3TEGT block. This result is consistent with previous work reporting that the alkyl chains are interdigitated and the methylene groups next to the ring interact with the aromatic rings of an adjacent stack.³⁸ The same self-assembly and micellization behavior are observed in THF-d₈/ CD₃OD solution (see SI.2.2, Figure S3). All the NMR results support a structure in which P3HT-*b*-P3TEGT self-assembles into polymeric core-shell nanomicelles with a double-layer architecture formed by a hydrophobic interior P3HT block surrounded by a hydrophilic exterior PEGT block. These observations are in good agreement with previous literature reports.^{34,39,40}

The successful self-assembly of P3HT-*b*-P3TEGT was confirmed by recording the absorption spectrum of both P3HT-*b*-P3TEGT and P3HT solutions after increasing the amount of methanol (Figure 3).⁴¹ In the case of P3HT (Figure 3a), one absorption peak at 435 nm was observed in THF, indicating that the polymer chains are well solvated in THF. In 30% methanol, the maximum shifts to 515 nm and additional absorption peaks at 555, and 610 nm appear. The new bands are attributed to aggregation in solution due to π - π stacking of the P3HT chains.⁴² As methanol ratio was further increased the low-energy peaks gradually increased, which is

indicative of increased intermolecular interactions between P3HT chains. The absorption spectra of P3HT-*b*-PTEG closely resemble to that of P3HT nanoparticles, with a shoulder peak around 425 nm, Figure 3b. The presence of this shoulder can be explained by the coexistence of both aggregated and coiled chains as previously reported in the literature.⁴³ Thus the main peak at around 425 nm in THF indicates that the two blocks of P3HT-*b*-P3TEGT are well solvated in THF. In 30% methanol, additional absorption peaks at 555, and 610 nm appear due to the improved π - π stacking of the P3HT block, which is the same as for the P3HT homopolymer.⁴² However, when the methanol ratio is further increased, these low-energy peaks increase gradually as a result of the formation of stable micelles with the hydrophilic shell outside, contrary to the P3HT homopolymer. Hence, this result proves that methanol, a poor solvent, induces the aggregation of P3HT, and as selective solvent for P3TEGT induces formation of stable nanomicelles of the block copolymer P3HT-*b*-P3TEGT with a core of P3HT block and a shell of P3TEGT block.

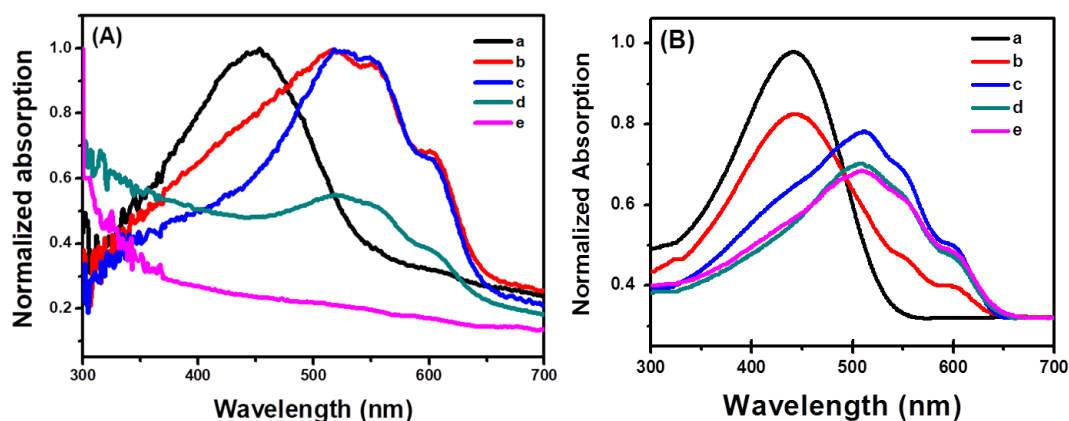


Figure 3. UV-vis spectrum of P3HT (A), and P3HT-*b*-P3TEGT (B) in THF solution with different methanol ratios: (a) 0%, (b) 30%, (c) 50%, (d) 70%, (e) 100%.

To examine the influence of the concentration of P3HT-*b*-P3TEGT materials and solvent composition on the micelle stability and micelle size distribution, three types of micelles were studied with different concentrations of P3HT-*b*-P3TEGT in THF/MeOH. Particle size distribution of P3HT-*b*-P3TEGT in THF/MeOH with different ratios, determined by DLS measurements, showed that aggregates with a monomodal size distribution were formed (see Section SI.2.2.2, and Table S1). The best stability was obtained for 1 mg/mL, and the hydrodynamic diameter of the

aggregates is 47 ± 8 nm when the methanol ratio is higher than 50%. TEM investigations showed that the P3HT-*b*-P3TEGT nanoparticles are spherical in shape with an average diameter of 50 nm and increase of diameter is observed for nanoparticles associated mannose Figure 4.

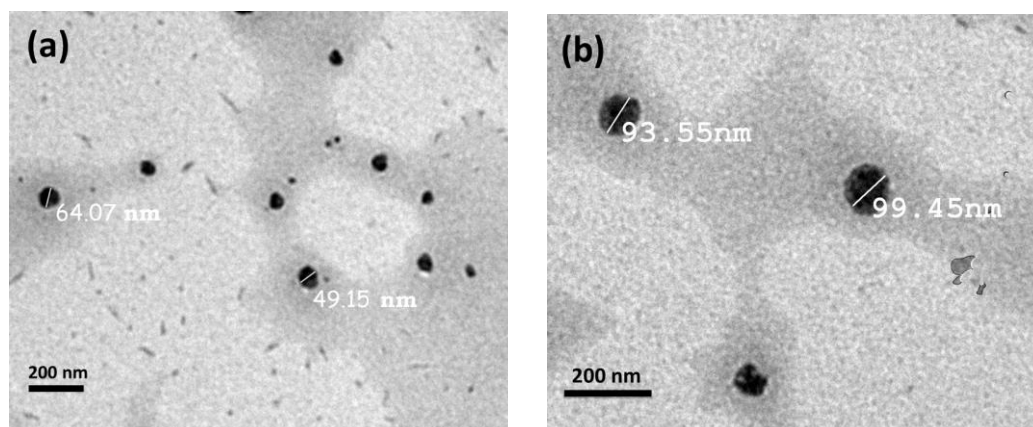


Figure 4. TEM image of P3HT-*b*-P3TEGT nanoparticles(a) and P3HT-*b*-P3TEGT functionalized with mannose (b)

3.2. Preparation of mannose-functionalized P3HT-*b*-P3TEGT nanomicelles

The objective is to generate a facile formulation of mannose-decorated nanomicelle by the self-assembly approach. Mannose could be coated during the formation of nanomicelles of P3HT-*b*-P3TEGT by using non-covalent hydrophilic-hydrophilic interactions between the TEG segments on the outer surface of the nanomicelles and the hydroxyl groups of the mannose (see SI.1.4 and Scheme 1). Mannose is a small molecule that is soluble in methanol, which is a selective solvent for the hydrophilic block of P3TEGT. Considering this fact, upon addition of a solution of mannose in methanol to P3HT-*b*-P3TEGT solution, mannose spontaneously organizes itself toward the hydrophilic part, and is physically adsorbed onto the outer surface of the nanomicelles. Mannose is then physically trapped within oxyethylene groups of TEG side-chains and stabilized via hydrophilic interaction between hydroxyl groups of mannose and oxyethylene side chain groups of TEG.⁴⁴ The self-assembly of copolymer in the presence of mannose and the formation of coated micelles are shown in SI.1.4, scheme S3. In order to assess the ability of mannose to functionalize the P3HT-*b*-P3TEGT and to coat the surface of the

nanoparticles, non-functionalized and mannose-functionalized films were analyzed by FTIR (Figure 5). The spectrum, taken after mannose conjugation and subsequently washed with DI water to remove excess mannose (Figure 5c), shows new vibrational bands (Figure 5b). The characteristic peaks of mannose related to the -OH group, a broad peak at 3330 cm^{-1} , and symmetric CH_2 stretching at $2843\text{--}2863\text{ cm}^{-1}$ were observed. This indicates stable immobilization of mannose by hydrogen bonding with oxygen (-O-) of oxyethylene group side-chains.

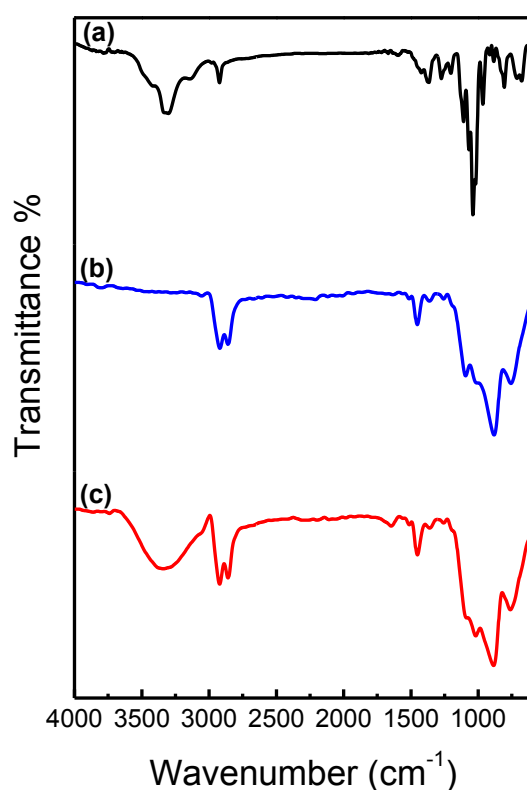


Figure 5. FTIR spectrum of (a) mannose, (b) P3HT-*b*-P3TEGT micelles, and (c) P3HT-*b*-P3TEGT/mannose micelles.

The water contact angles of P3HT, P3HT-*b*-P3TEGT, and P3HT-*b*-P3TEGT/mannose thin films were measured to assess the wettability of the surfaces (Figure 6). The contact angle of 33° shows that P3HT-*b*-P3TEGT film has a hydrophilic surface (Figure 6b), compared to the hydrophobic surface of P3HT with a contact angle of 107° (Figure 6a). This explains that upon evaporation of solvent the TEG side-chains of the P3TEGT block would spontaneously migrate vertically to the

active layers that enhance wettability and hydrophilicity. For mannose-functionalized P3HT-*b*-P3TEGT nanomicelles (Figure 5c), the contact angle decreases dramatically to a value less than 20° compared to 33° for the non-functionalized copolymer. This means that the incorporation of mannose into the copolymer increases the wettability of its surface. Further characterizations are necessary to investigate the homogeneity and intimate mixing of mannose and P3HT-*b*-P3TEGT on thin film.

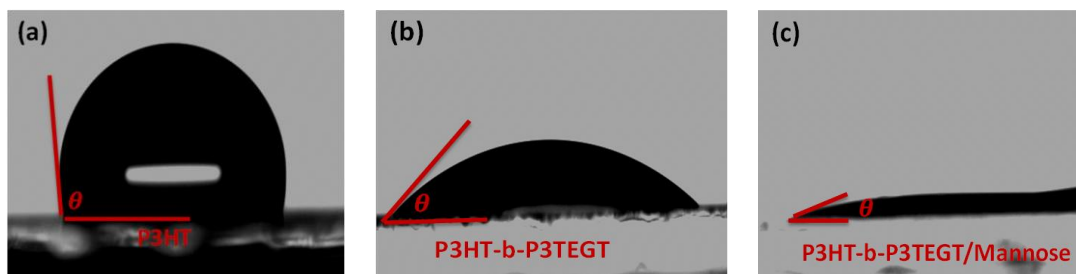


Figure 6. Static contact angle of water droplet on glass substrate cast with: (a) P3HT (b) P3HT-*b*-P3TEGT, and (c) P3HT-*b*-P3TEGT/mannose.

One of the motivations of this work is to validate our idea of detecting bacteria with a unlabeled biosensor using mannose-functionalized core-shell nanoparticles. The attachment of the bacteria to the glyco-surface through lectin-mannose interaction is well known.^{45,17} Various mannose-functionalized glycol nanoparticles have been shown to specifically bind to FimH adhesion of type 1 pili in *E. coli*.⁴⁶ Thus, we moved to the study of the scope and limitations of these mannose-decorated P3HT-*b*-P3TEGT nanoparticles for sensing bacteria.

The surface properties of biosensors are crucial issues for non-specific adsorption of proteins and microorganisms at bio-interfaces in biological environments.^{47, 48} Therefore, the development of biosensing interfaces that combine high sensitivity and antifouling ability is essential to expanding the practical applicability of biosensors to allow reliable measurements. Immobilizing oligo(ethylene oxide) groups is one of the most commonly used approach to suppress micro-organism and protein attachment to a surface in certain configurations.^{49,50} Indeed, as previously discussed, the copolymers self-assembled into core-shell micelles with oligo(ethylene oxide) group-enriched surface, such layers enhance wettability and hydrophilicity of film surface, therefore they are very efficient in preventing non-specific attachment of bacteria. Therefore, the antifouling behavior of P3HT-*b*-P3TEGT was tested. The properties of polymeric surfaces and their effect on

E. coli attachment were first investigated by optical microscopy and then by SEM. Optical microscope images of glass substrate modified film after incubation with 1.0×10^7 CFU/mL *E. coli*. P3HT film (Figure 7a) show bacterial attachment corresponding to the non-specific interaction of the surface. While P3HT-*b*-P3TEGT film (Figure 7b) shows no bacterial cell attachment. This result is related to the antifouling surface provided by the association of water within TEG side-chains, leading to the exclusion of biomolecules from the surface. The TEG chain orientation of the P3TEGT block on the surface would be responsible of the antifouling properties. This antifouling polymeric film is an ideal surface to modify with a suitable bioreceptor that could selectively interact with the target without non-specific interaction of other types of bacteria. In the case of the film of mannose-coated P3HT-*b*-P3TEGT (Figure 6c), the image shows attachment of bacterial cells to the surface. This is due to Fim H lectin in the bacterial surface able to bind to mannose on the surface of P3HT-*b*-P3TEGT film. Thus the results obtained by optical microscopy highlight the fact that *E. coli* attachment to polymeric surfaces is most affected by the surface energy, as determined by the water contact angle and the presence of bioreceptors such as mannose on the surface.

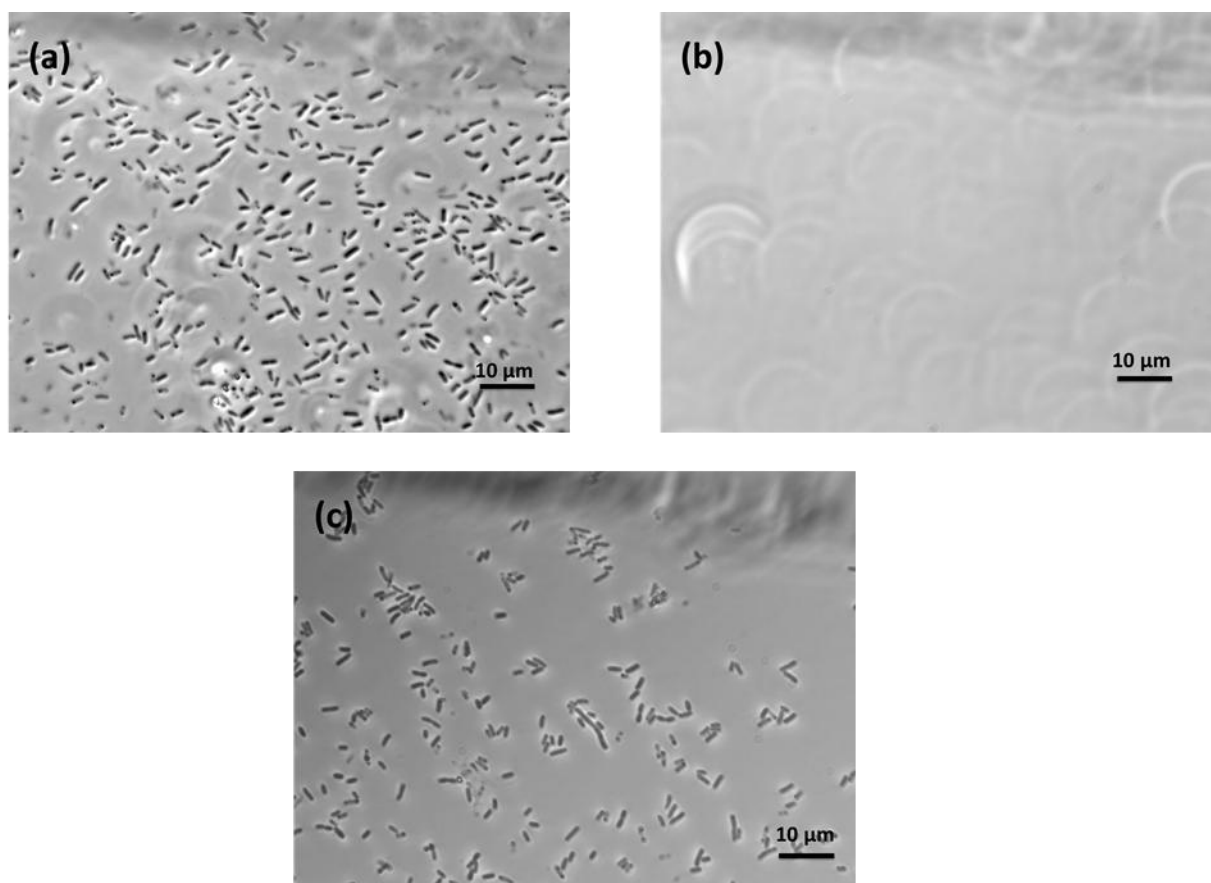


Figure 7. Optical microscopy images of glass substrate modified by: (a) P3HT, (b) P3HT-*b*-P3TEGT, and (c) P3HT-*b*-P3TEGT/mannose images **after incubation with *E. Coli* (1.0×10^7 CFU/mL) during 1h and washing step.**

SEM was used to assess the antifouling properties of the P3HT-*b*-P3TEGT film and to confirm the attachment of bacteria to the mannose-modified P3HT-*b*-P3TEGT film. As shown in Figure 8, when a P3HT-*b*-P3TEGT film was incubated with a solution of *E. coli* (1.0×10^7 CFU/mL), no bacteria were attached to the surface of the film. However, after exposing the substrate surface, P3HT-*b*-P3TEGT/mannose film, to the same concentration of *E. coli*, the SEM image clearly shows the attachment of *E. coli* to the surface of the film (Figure 8b). This means that mannose-decorated P3HT-*b*-P3TEGT offers an ideal bio-interface to selectively fix *E. coli*, thanks to mannose-lectin binding interaction.

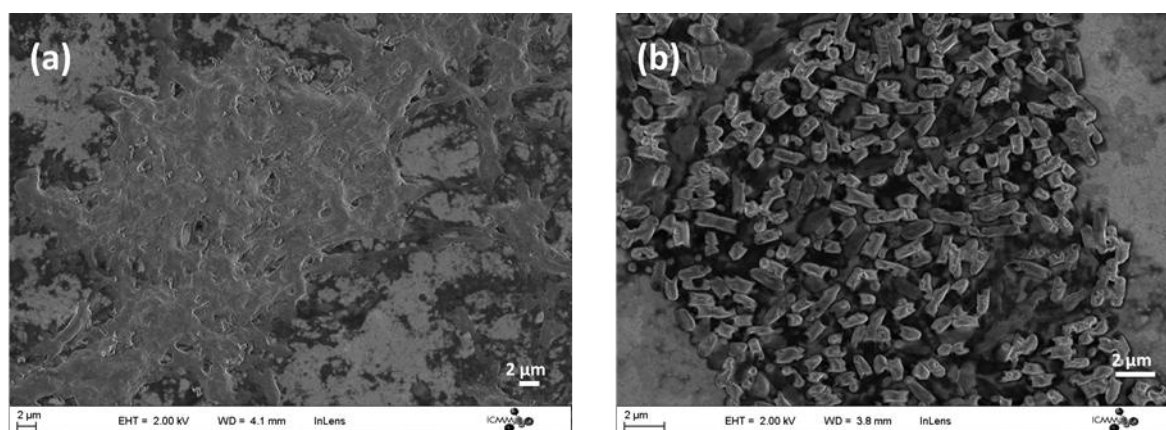


Figure 8. SEM images after incubation with *E. coli* (1.0×10^7 CFU/mL): (a) P3HT-*b*-P3TEGT film, (b) P3HT-*b*-P3TEGT/mannose film.

3.4. Electrochemical characterization and *E. coli* detection

Electrochemical characterization of P3HT and P3HT-*b*-P3TEGT modified GCE was studied by CV and EIS in PBS buffer. CV curves (Figure S4A) show that P3HT does not have any electrochemical activity while P3HT-*b*-P3TEGT shows a clear reversible oxidation peak corresponding to the doping/de-doping of conjugated polymers.⁵⁰ **Both polymers show good reversible redox features in organic solvents, demonstrating doping dedoping process (Figure S4B). The absence of the electrochemical activity and redox peaks of P3HT in aqueous solution has been reported in the literature and interpreted as a consequence of hydrophobicity of the alkyl chains, which limits the transport of ionic species within the P3HT.⁵¹** This demonstrates that the TEG side-chain improves the wettability of the polymer backbone in aqueous media and leads to an improvement in electronic and ionic

transfer. The same behaviour was previously reported for conjugated polythiophene, where the enhancement of the hydrophilic character improves ionic transport and doping/de-doping in aqueous media.³³ The redox potential of P3HT-*b*-P3TEGT, which corresponds to the average of the oxidation and reduction potentials, is 0.4V/Ag/AgCl. This potential is higher than that reported for polythiophene substituted by a TEG side-chain⁵⁰ which could be related to the presence of the hydrophobic P3HT block in the copolymer. The electrochemistry results are in good agreement with that reported for oligo(ethylene glycol)substituted conjugated polymers, where glycol side chains have shown to facilitate polymer swelling and ions transport in conjugated polymers, allowing ions to penetrate into the bulk during electrochemical redox reactions in aqueous electrolytes.

EIS measurements were performed in PBS solution without a redox marker, to investigate the electrical properties of the electroactive layer. This was performed in a potential range where the current is small, to ensure the stability of the measurement. The potential chosen is -0.4 V vs. Ag/AgCl, where the polymer is in its semiconducting state. Nyquist plots were recorded for films of P3HT/GCE and to P3HT-*b*-P3TEGT/GCE (Figure S4B). A well semicircle was obtained with both polymers and nanomicelles. In the case of P3HT-*b*-P3TEGT (Figure S4B, curve b) the higher diameter of the semicircle is related to charge transfer resistance of the electronic transfer from the polymer to electrode.. The fitting data were performed with an equivalent circuit model where the electronic properties of the layers are represented by a charge transfer resistance (R_{ct}) in parallel with a capacitance and in series with the resistance of the solution (R_s). In both copolymers and film formed with nanomicelle the capacitance was replaced by a constant phase element (CPE), which underlines the inhomogenous charge distribution in the film (see Section SI.3 of SI, Table S2 for fitting data). In the case of the P3HT-*b*-P3TEGT/GCE and nanomicelle Warburg impedance is observed with is related to the diffusion of ions and demonstrates the ability of the copolymer to diffusion process. Both films of polymer and copolymer have the same R_{ct} value, however the film formed with nanomicelle shows a small decrease of R_{ct} which demonstrates their large ability for ionic and electronic transfer. The capacitance behaviour is higher in the case of copolymer which could be related to swelling and ionic exchange in water solution.⁵² From these results, It is difficult to quantify the contribution of ionic and electronic transfer in copolymer and nanomicelle, however It is clear that the introduction of the

TEG chains in P3HT-*b*-P3TEGT does not affect the electronics properties of the polymers **but improves the ionic transfer**. Thus, the interfacial properties changed due to the enhanced diffusion process in the case of the copolymers. This demonstrates that the swelling of P3HT-*b*-P3TEGT on the surface allows higher diffusion process thanks to hydrophilic TEG side-chain.

The detection of *E. coli* via binding of P3HT-*b*-P3TEGT/mannose-modified GCE was characterized by EIS as one of the most promising methods for studying the interactions of bacteria with bioactive surfaces.⁵³ The EIS technique has become increasingly popular in a variety of bacteria biosensing applications because it offers several advantages, such as simplicity, is label-free, has high sensitivity, and can serve as way to interface bio-recognition events and signal transduction.⁵⁴ Here, attachment of bacteria to the electrode surface is detected without using a redox indicator and is directly proportional to the change in the electrical properties of the conjugated polymer.^{17,25}

The stability of the EIS signal was firstly analyzed by using various P3HT-*b*-P3TEGT/mannose films after optimization of the experimental conditions of film formation, such as the ratio of P3HT-*b*-P3TEGT to mannose, the annealing temperature, and time. (For additional details see section SI.3.2, Figure S5 and SI.4.1, Figure S6.) The optimal conditions provide a homogenous sensing layer with good stability and reproducibility.

The analysis of the response signal was then measured after the attachment of bacteria and a washing step to conserve only bacteria attached to the surface through pili/mannose interactions. Nyquist plots were recorded under the same conditions as demonstrated previously in a large frequency range at a potential where P3HT-*b*-P3TEGT is in its semi-conducting state before and after incubation of various concentrations of bacteria (Figure 9a). An increase in the width of the semicircle after bacterial attachment, depending of the concentration incubated, is observed. This result underlines that the attachment of bacteria affects the electrical properties of the sensing layer, such as charge transfer resistance and capacitance. This behavior is generally observed when large biomolecules are attached to the surface of the electrode, thus reducing the ionic and electronic transfer efficiency. The impedance data were fitted into an equivalent circuit model and the R_{ct} obtained after the immobilization of bacteria was used to construct the calibration curve for concentrations of bacteria from 10^3 CFU/mL to 10^7 CFU/mL (Table S4 in SI). The

calibration curve shows a dynamic variation with the logarithm of the bacteria concentration (Figure 9b), and the detection limit based on S/N 3 was calculated to be 500 CFU/mL. This limit of detection is very good compared to the literature reporting the use of redox-active conjugated polymers as electrode material for bacteria detection, see table S5 in SI.

The selectivity of the sensor was studied with a Gram(+) bacterium, *L. acidophilus* (ATCC 4356). This bacterium was chosen as it is reported to have no affinity for mannose and no binding capability.⁵⁵ The EIS response was recorded with the P3HT-*b*-P3TEGT/mannose film after incubation of 10^5 CFU/mL of *L. acidophilus* (Figure 9c). There is no variation of the EIS after *L. acidophilus* incubation (curves a and b), while the same modified electrode shows a large variation in the Nyquist plot when the two bacteria are mixed (curve c). This result underlines that P3HT-*b*-P3TEGT/mannose selectively detects *E. coli* even in the presence of other types of bacteria. Figure 9d displays the histogram response obtained with the two bacteria and shows clearly the selectivity of the biosensor.

The reproducibility of the biosensor was evaluated with successive measurements of *E. coli* at concentrations from 10^3 to 10^7 CFU/mL for three different P3HT-*b*-P3TEGT/mannose-modified electrodes. The mean relative standard deviation (RSD) of 4.1% demonstrates the reproducibility of the biosensors. This reproducibility could be improved by using other deposition methods, such as spin-coating or the doctor blade technique.

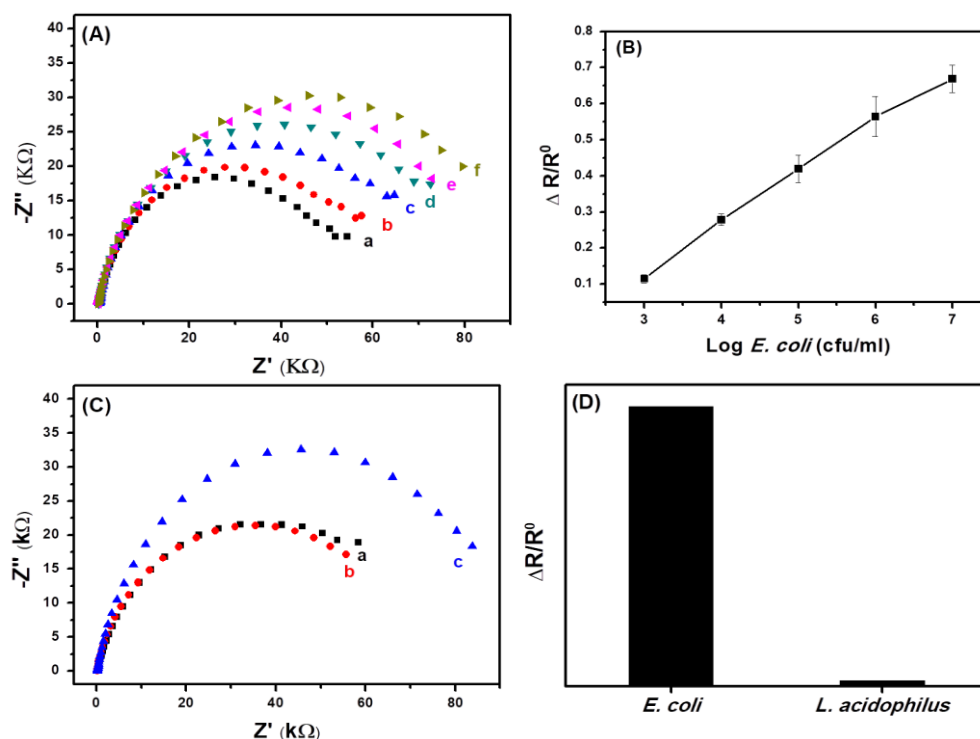


Figure 9. (A) Nyquist diagrams of a P3HT-b-P3TEGT/mannose modified GCE obtained with increasing concentrations of *E. coli* in PBS: (a) 10^3 CFU/mL, (b) 10^4 CFU/mL, (c) 10^5 CFU/mL, (d) 10^6 CFU/mL, (e) 10^7 CFU/mL, (f) (B) Calibration curve; (C) Nyquist plot for test selectivity of P3HT-b-P3TEGT/mannose modified GCE for: (c) *E. coli* compared to (b) *L. acidophilus* and (a) PBS, (D) Histogram of average variation between the two bacteria.

3.5 Detection in real sample

Drinking water and Nile water were tested as real samples to determine the performance of the biosensor in real applications using a standard addition method. A sample of drinking tap water (pH 6.7) was previously treated with a 0.22 μm syringe filter to remove all bacterial cell contaminants, and then three concentrations, 10^4 , 10^5 and 10^6 CFU/mL, of *E. coli* were inoculated. Nyquist plots were measured and the average variation of the Rct was calculated. The recovery was obtained by comparing the value added and that measured. The recovery of measured *E. coli* in tap water (Table 1) is between 81 to 95%. This demonstrates the ability of the biosensors to measure the bacteria in tap water even at low values. The mean RSD is 2.3%.

Table 1. Analysis of spiked tap water for the determination of *E. coli*.

Sample	added	Measured	Recovery	RSD (n=3)
1	10^4	9.5×10^3	95 %	4.2%
2	10^5	8.7×10^4	87 %	0.7%
3	10^6	8.1×10^5	81 %	2.1%

An experiment with contaminated water was performed to test the ability of the sensor for real-sample measurement. For this purpose water from the Nile (sampling site: Beni-suef, Egypt) was collected and not treated. Nile water already contains bacteria as it is purified by the conventional plate culture method (see SI, Figure S8). To determine the amount of bacteria in a sample of Nile water, a blank test was first recorded to eliminate the matrix effect. This was obtained by measuring the EIS with a Nile sample after filtration through a 0.22 μm filter to remove all micro-organisms. The curve obtained for the blank test was compared with that for an untreated sample of Nile water (See SI. 4.2, Figure S8). The variation allows to calculate the concentration of bacteria in the Nile. The average variation of Rct allows to calculate the quantity of bacteria attached, which is 10^6 CFU/mL. This result is of

the same order of magnitude as that obtained by the conventional method based on culture and counting (see SI.4.2).

4. Conclusion

This work demonstrates the feasibility of using solution-processable glycosylated nanoparticle-based materials in impedimetric sensors for detecting bacteria. These glycosylated nanoparticles are promising materials for the fabrication of label-free biosensors for the detection of whole bacterial cells, with the following advantages. First, the CP nanomicelles decorated with mannose are readily made by direct blending without any pre-treatment or complicated chemistry, making this a very simple and low-cost functionalization technique. Second, the presence of the oligoethylene glycol side-chain in the P3TEGT block suppresses non-specific bacterial adhesion, which favors selectivity toward mannose-binding bacteria and enhances the P3HT-*b*-P3TEGT/mannose biosensor performance. Third, mannose, as small carbohydrate molecule, physically trapped within the film provides larger surface area for binding the target proteins of *E. coli*. Moreover, the use of the amphiphilic CP approach achieves label-free and reagentless transduction of the biological binding events into electric signals by EIS, where increasing concentrations of the bacteria increase the signal. Analysis of the impedimetric parameters shows that the biosensor has significant sensitivity and specificity for the detection of *E. coli* BL21 without using a redox marker, with a detection limit of 500 CFU/mL and a linear range from 10^3 to 10^7 CFU/mL. The biosensor can be used as a continuous response sensor until saturation is reached at 10^7 CFU/mL. The biosensor enables accurate determination of *E. coli* concentrations, even under conditions of contaminated tap and Nile water.

Acknowledgments

N. E. G. acknowledges grants No from the Ministry of Higher Education in Egypt. A.Y. thanks ANR-16-CE07-0024 (GATE), R.S. thanks the China Scholarship Council for a PhD fellowship (No.201808070090) and H.K.Y. thanks the MAEF for the PHC project (No39382RE). Authors tanks to Pr. John;;; for English revision of the manuscript.

References

- (1) Moldenhauer, J. Overview of Rapid Microbiological Methods. In *Principles of Bacterial Detection: Biosensors, Recognition Receptors and Microsystems*; Zourob, M.; Elwary, S.; Turner, A., Eds.; Springer New York: New York, NY, 2008; pp 49-79.
- (2) Mobed, A.; Baradaran, B.; Guardia, M. d. I.; Agazadeh, M.; Hasanzadeh, M.; Rezaee, M. A.; Mosafer, J.; Mokhtarzadeh, A.; Hamblin, M. R. Advances in detection of fastidious bacteria: From microscopic observation to molecular biosensors. *TrAC Trends in Analytical Chemistry* **2019**, *113*, 157-171, DOI: <https://doi.org/10.1016/j.trac.2019.02.012>.
- (3) Zhao, Y. W.; Wang, H. X.; Jia, G. C.; Li, Z. Application of Aptamer-Based Biosensor for Rapid Detection of Pathogenic Escherichia coli. *Sensors* **2018**, *18* (8), DOI: 10.3390/s18082518.
- (4) Ahmed, A.; Rushworth, J. V.; Hirst, N. A.; Millner, P. A. Biosensors for Whole-Cell Bacterial Detection. *Clinical Microbiology Reviews* **2014**, *27* (3), 631-646, DOI: 10.1128/cmr.00120-13.
- (5) Furst, A. L.; Francis, M. B. Impedance-Based Detection of Bacteria. *Chemical Reviews* **2019**, *119* (1), 700-726, DOI: 10.1021/acs.chemrev.8b00381.
- (6) Pourakbari, R.; Shadjou, N.; Yousefi, H.; Isildak, I.; Yousefi, M.; Rashidi, M.-R.; Khalilzadeh, B. Recent progress in nanomaterial-based electrochemical biosensors for pathogenic bacteria. *Microchimica Acta* **2019**, *186* (12), 820, DOI: 10.1007/s00604-019-3966-8.
- (7) Muniandy, S.; Teh, S. J.; Thong, K. L.; Thiha, A.; Dinshaw, I. J.; Lai, C. W.; Ibrahim, F.; Leo, B. F. Carbon Nanomaterial-Based Electrochemical Biosensors for Foodborne Bacterial Detection. *Critical Reviews in Analytical Chemistry* **2019**, *49* (6), 510-533, DOI: 10.1080/10408347.2018.1561243.
- (8) Szunerits, S.; Boukherroub, R. Graphene-based biosensors. *Interface Focus* **2018**, *8* (3), 20160132, DOI: doi:10.1098/rsfs.2016.0132.
- (9) Hackett, A. J.; Malmström, J.; Travas-Sejdic, J. Functionalization of conducting polymers for biointerface applications. *Progress in Polymer Science* **2017**, *70*, 18-33, DOI: <https://doi.org/10.1016/j.progpolymsci.2017.03.004>.
- (10) Naseri, M.; Fotouhi, L.; Ehsani, A. Recent Progress in the Development of Conducting Polymer-Based Nanocomposites for Electrochemical Biosensors Applications: A Mini-Review. *The Chemical Record* **2018**, *18* (6), 599-618, DOI: 10.1002/tcr.201700101.
- (11) Zeglio, E.; Rutz, A. L.; Winkler, T. E.; Malliaras, G. G.; Herland, A. Conjugated Polymers for Assessing and Controlling Biological Functions. *Advanced Materials* **2019**, *31* (22), 1806712, DOI: 10.1002/adma.201806712.
- (12) Inal, S.; Rivnay, J.; Sui, A.-O.; Malliaras, G. G.; McCulloch, I. Conjugated Polymers in Bioelectronics. *Accounts of Chemical Research* **2018**, *51* (6), 1368-1376, DOI: 10.1021/acs.accounts.7b00624.
- (13) Hackett, A.; Strover, L.; Baek, P.; Malmstrom, J.; Travas-Sejdic, J. Polymer-Grafted Conjugated Polymers as Functional Biointerfaces. In *Conjugated Polymers for Biological and Biomedical Applications*; Liu, B., Ed.; Wiley- VCH Verlag GmbH & Co: 2018.
- (14) Pan, H. M.; Gonuguntla, S.; Li, S.; Trau, D. Conjugated Polymers for Biosensor Devices II. In *Comprehensive Biomaterials II*; Ducheyne, P., Ed.; Elsevier: 2017; pp 716-754.
- (15) Jelinek, R.; Kolusheva, S. Carbohydrate Biosensors. *Chemical Reviews* **2004**, *104* (12), 5987-6016, DOI: 10.1021/cr0300284.

- (16) Tsakama, M.; Ma, X. C.; He, Y. H.; Chen, W. H.; Dai, X. F. A Simple Mannose-Coated Poly (p-Phenylene Ethynylene) for Qualitative Bacterial Capturing. *Molecules* **2018**, *23* (8), DOI: 10.3390/molecules23082056.
- (17) Zeng, X.; Qu, K.; Rehman, A. Glycosylated Conductive Polymer: A Multimodal Biointerface for Studying Carbohydrate–Protein Interactions. *Accounts of Chemical Research* **2016**, *49* (9), 1624-1633, DOI: 10.1021/acs.accounts.6b00181.
- (18) Wang, D.; Gong, X.; Heeger, P. S.; Rininsland, F.; Bazan, G. C.; Heeger, A. J. Biosensors from conjugated polyelectrolyte complexes. *Proceedings of the National Academy of Sciences* **2002**, *99* (1), 49-53, DOI: 10.1073/pnas.012581399.
- (19) Pu, K.-Y.; Liu, B. A Multicolor Cationic Conjugated Polymer for Naked-Eye Detection and Quantification of Heparin. *Macromolecules* **2008**, *41* (18), 6636-6640, DOI: 10.1021/ma801269n.
- (20) Duarte, A.; Chworos, A.; Flagan, S. F.; Hanrahan, G.; Bazan, G. C. Identification of Bacteria by Conjugated Oligoelectrolyte/Single-Stranded DNA Electrostatic Complexes. *Journal of the American Chemical Society* **2010**, *132* (36), 12562-12564, DOI: 10.1021/ja105747b.
- (21) Baek, M.-G.; Stevens, R. C.; Charych, D. H. Design and Synthesis of Novel Glycopolythiophene Assemblies for Colorimetric Detection of Influenza Virus and E. coli. *Bioconjugate Chemistry* **2000**, *11* (6), 777-788, DOI: 10.1021/bc000026f.
- (22) Liu, Y.; Ogawa, K.; Schanze, K. S. Conjugated polyelectrolytes as fluorescent sensors. *Journal of Photochemistry and Photobiology C-Photochemistry Reviews* **2009**, *10* (4), 173-190, DOI: 10.1016/j.jphotochemrev.2009.10.003.
- (23) Gondran, C.; Fort, S.; Cosnier, S. Electrogenated poly(pyrrole-lactosyl) and poly(pyrrole-3'-sialyllactosyl) interfaces: toward the impedimetric detection of lectins. *Frontiers in Chemistry* **2013**, *1* (10), DOI: 10.3389/fchem.2013.00010.
- (24) Qu, K.; Kondengaden, S. M.; Li, J.; Wang, X.; Sevilla, M. D.; Li, L.; Zeng, X. Carbohydrate-functionalized polythiophene biointerface: design, fabrication, characterization and application for protein analysis. *Applied Surface Science* **2019**, *486*, 561-570, DOI: <https://doi.org/10.1016/j.apsusc.2019.04.231>.
- (25) Ma, F.; Rehman, A.; Liu, H.; Zhang, J.; Zhu, S.; Zeng, X. Glycosylation of Quinone-Fused Polythiophene for Reagentless and Label-Free Detection of E. coli. *Analytical Chemistry* **2015**, *87* (3), 1560-1568, DOI: 10.1021/ac502712q.
- (26) Gao, M.; Li, L.; Song, Y. Inkjet printing wearable electronic devices. *Journal of Materials Chemistry C* **2017**, *5* (12), 2971-2993, DOI: 10.1039/C7TC00038C.
- (27) Gonzalez-Macia, L.; Morrin, A.; Smyth, M. R.; Killard, A. J. Advanced printing and deposition methodologies for the fabrication of biosensors and biodevices. *Analyst* **2010**, *135* (5), 845-867, DOI: 10.1039/b916888e.
- (28) Xu, T. D. Conjugated Polymer Nanoparticles and Semiconducting Polymer Dots for Molecular Sensing and In Vivo and Cellular Imaging. In *Conjugated Polymers for Biological and Biomedical Applications*; Liu, B., Ed.; Wiley- VCH Verlag GmbH & Co: 2018; pp 59-85.
- (29) Song, I. Y.; Kim, J.; Im, M. J.; Moon, B. J.; Park, T. Synthesis and Self-Assembly of Thiophene-Based All-Conjugated Amphiphilic Diblock Copolymers with a Narrow Molecular Weight Distribution. *Macromolecules* **2012**, *45* (12), 5058-5068, DOI: 10.1021/ma300771g.
- (30) Urien, M.; Erothu, H.; Cloutet, E.; Hiorns, R. C.; Vignau, L.; Cramail, H. Poly(3-hexylthiophene) Based Block Copolymers Prepared by “Click” Chemistry. *Macromolecules* **2008**, *41* (19), 7033-7040, DOI: 10.1021/ma800659a.
- (31) Dissanayake, D. S.; Sheina, E.; Biewer, M. C.; McCullough, R. D.; Stefan, M. C. Determination of absolute molecular weight of regioregular poly(3-hexylthiophene)

- by ¹H-NMR analysis. *Journal of Polymer Science Part A: Polymer Chemistry* **2017**, 55 (1), 79-82, DOI: 10.1002/pola.28354.
- (32) Jain, S.; Bates, F. S. On the Origins of Morphological Complexity in Block Copolymer Surfactants. *Science* **2003**, 300 (5618), 460-464, DOI: 10.1126/science.1082193.
- (33) Reichstein, P. M.; Gödrich, S.; Papastavrou, G.; Thelakkat, M. Influence of Composition of Amphiphilic Double-Crystalline P3HT-b-PEG Block Copolymers on Structure Formation in Aqueous Solution. *Macromolecules* **2016**, 49 (15), 5484-5493, DOI: 10.1021/acs.macromol.6b01305.
- (34) Kim, J.; Song, I. Y.; Park, T. Polymeric vesicles with a hydrophobic interior formed by a thiophene-based all-conjugated amphiphilic diblock copolymer. *Chemical Communications* **2011**, 47 (16), 4697-4699, DOI: 10.1039/C1CC10700C.
- (35) Markowicz, M.; Szymański, P.; Ciszewski, M.; Kłys, A.; Mikiciuk-Olasik, E. Evaluation of poly(amidoamine) dendrimers as potential carriers of iminodiacetic derivatives using solubility studies and 2D-NOESY NMR spectroscopy. *Journal of Biological Physics* **2012**, 38 (4), 637-656, DOI: 10.1007/s10867-012-9277-5.
- (36) Righetti, P. G. Biomacromolecules: Introduction to structure, Function and Informatics. By C. Stan Tsai. *Biotechnology Journal* **2008**, 3 (6), 825-826, DOI: 10.1002/biot.200890064.
- (37) Higashihara, T.; Ohshimizu, K.; Ryo, Y.; Sakurai, T.; Takahashi, A.; Nojima, S.; Ree, M.; Ueda, M. Synthesis and characterization of block copolythiophene with hexyl and triethylene glycol side chains. *Polymer* **2011**, 52 (17), 3687-3695, DOI: <https://doi.org/10.1016/j.polymer.2011.06.037>.
- (38) Parenti, F.; Tassinari, F.; Libertini, E.; Lanzi, M.; Mucci, A. π -Stacking Signature in NMR Solution Spectra of Thiophene-Based Conjugated Polymers. *ACS Omega* **2017**, 2 (9), 5775-5784, DOI: 10.1021/acsomega.7b00943.
- (39) Tu, G.; Li, H.; Forster, M.; Heiderhoff, R.; Balk, L. J.; Sigel, R.; Scherf, U. Amphiphilic Conjugated Block Copolymers: Synthesis and Solvent-Selective Photoluminescence Quenching. *Small* **2007**, 3 (6), 1001-1006, DOI: 10.1002/smll.200600351.
- (40) Jiao, H.-F.; Wang, X.; Yao, K.; Chen, P.; Jia, Z.; Peng, Z.; Li, F. Self-assembly of all-conjugated block copolymer nanoparticles with tailoring size and fluorescence for live cell imaging. *Journal of Materials Chemistry B* **2016**, 4 (48), 7882-7887, DOI: 10.1039/C6TB02211A.
- (41) Yu, Z.; Yan, H.; Lu, K.; Zhang, Y.; Wei, Z. Self-assembly of two-dimensional nanostructures of linear regioregular poly(3-hexylthiophene). *RSC Advances* **2012**, 2 (1), 338-343, DOI: 10.1039/C1RA00833A.
- (42) Jo, G.; Jung, J.; Chang, M. Controlled Self-Assembly of Conjugated Polymers via a Solvent Vapor Pre-Treatment for Use in Organic Field-Effect Transistors. *Polymers* **2019**, 11 (2), DOI: 10.3390/polym11020332.
- (43) Scharsich, C.; Lohwasser, R. H.; Sommer, M.; Asawapirom, U.; Scherf, U.; Thelakkat, M.; Neher, D.; Köhler, A. Control of aggregate formation in poly(3-hexylthiophene) by solvent, molecular weight, and synthetic method. *Journal of Polymer Science Part B: Polymer Physics* **2012**, 50 (6), 442-453, DOI: 10.1002/polb.23022.
- (44) Zhou, B.; Hu, X.; Zhu, J.; Wang, Z.; Wang, X.; Wang, M. Release properties of tannic acid from hydrogen bond driven antioxidative cellulose nanofibrous films. *International Journal of Biological Macromolecules* **2016**, 91, 68-74, DOI: <https://doi.org/10.1016/j.ijbiomac.2016.05.084>.

- (45) Disney, M. D.; Zheng, J.; Swager, T. M.; Seeberger, P. H. Detection of Bacteria with Carbohydrate-Functionalized Fluorescent Polymers. *Journal of the American Chemical Society* **2004**, *126* (41), 13343-13346, DOI: 10.1021/ja047936i.
- (46) Kheireddine, E.-B.; Xuefei, H. Glyco-nanomaterials: Translating Insights From the "Sugar-Code" to Biomedical Applications *Current Medicinal Chemistry* **2011**, *18* (14), 2060-2078, DOI: <http://dx.doi.org/10.2174/092986711795656144>.
- (47) Lichtenberg, J. Y.; Ling, Y.; Kim, S. Non-Specific Adsorption Reduction Methods in Biosensing. *Sensors* **2019**, *19* (11), DOI: 10.3390/s19112488.
- (48) Wu, J.-G.; Chen, J.-H.; Liu, K.-T.; Luo, S.-C. Engineering Antifouling Conducting Polymers for Modern Biomedical Applications. *ACS Applied Materials & Interfaces* **2019**, *11* (24), 21294-21307, DOI: 10.1021/acsami.9b04924.
- (49) Ista, L. K.; Fan, H.; Baca, O.; López, G. P. Attachment of bacteria to model solid surfaces: oligo(ethylene glycol) surfaces inhibit bacterial attachment. *FEMS Microbiology Letters* **1996**, *142* (1), 59-63, DOI: 10.1111/j.1574-6968.1996.tb08408.x.
- (50) Sanni, O.; Chang, C.-Y.; Anderson, D. G.; Langer, R.; Davies, M. C.; Williams, P. M.; Williams, P.; Alexander, M. R.; Hook, A. L. Bacterial Attachment to Polymeric Materials Correlates with Molecular Flexibility and Hydrophilicity. *Advanced Healthcare Materials* **2015**, *4* (5), 695-701, DOI: 10.1002/adhm.201400648.
- (51) Skompska, M.; Szkurlat, A.; Kowal, A.; Szklarczyk, M. Spectroelectrochemical and AFM Studies of Doping–Undoping of Poly(3-hexylthiophene) Films in Propylene Carbonate and Aqueous Solutions of LiClO₄. *Langmuir* **2003**, *19* (6), 2318-2324, DOI: 10.1021/la0261850.
- (52) Schmode, P.; Savva, A.; Kahl, R.; Ohayon, D.; Meichsner, F.; Dolynchuk, O.; Thurn-Albrecht, T.; Inal, S.; Thelakkat, M. The Key Role of Side Chain Linkage in Structure Formation and Mixed Conduction of Ethylene Glycol Substituted Polythiophenes. *ACS Applied Materials & Interfaces* **2020**, *12* (11), 13029-13039, DOI: 10.1021/acsami.9b21604.
- (53) Wang, Y. X.; Ye, Z. Z.; Ying, Y. B. New Trends in Impedimetric Biosensors for the Detection of Foodborne Pathogenic Bacteria. *Sensors* **2012**, *12* (3), 3449-3471, DOI: 10.3390/s120303449.
- (54) Yang, H.; Zhou, H.; Hao, H.; Gong, Q.; Nie, K. Detection of Escherichia coli with a label-free impedimetric biosensor based on lectin functionalized mixed self-assembled monolayer. *Sensors and Actuators B: Chemical* **2016**, *229*, 297-304, DOI: <https://doi.org/10.1016/j.snb.2015.08.034>.
- (55) Holst, B.; Glenting, J.; Holmstrøm, K.; Israelsen, H.; Vrang, A.; Antonsson, M.; Ahrné, S.; Madsen, S. M. Molecular Switch Controlling Expression of the Mannose-Specific Adhesin, Msa, in Lactobacillus plantarum. *Applied and Environmental Microbiology* **2019**, *85* (10), e02954-18, DOI: 10.1128/aem.02954-18.

Table of content :